

# Interaction of multiple atmospheric-pressure micro-plasma jets in small arrays: He/O<sub>2</sub> into humid air

Natalia Yu Babaeva and Mark J Kushner<sup>1</sup>

Department of Electrical Engineering and Computer Science, University of Michigan, 1301 Beal Ave., Ann Arbor, MI 48109-2122, USA

E-mail: [nbabaeva@umich.edu](mailto:nbabaeva@umich.edu) and [mjkush@umich.edu](mailto:mjkush@umich.edu)

Received 18 August 2013, revised 6 December 2013

Accepted for publication 6 December 2013

Published 10 January 2014

## Abstract

Arrays of atmospheric-pressure plasma jets are being considered as a means to increase the area being treated in surface modification and in plasma medicine in particular. A unique challenge of scaling plasma jet arrays is that individual plasma jets in an array tend to interact with each other, which can lead to quenching of some individual jets. To investigate these potential interactions, a computational study of one-, two- and three-tube arrays of micro-plasma jet arrays was performed. An atmospheric-pressure He/O<sub>2</sub> = 99.8/0.2 mixture was flowed through the tubes into humid room air. We found that the jets interact through electrostatic, hydrodynamic and photolytic means. The hydrodynamic interactions result from the merging of individual He channels emerging from individual tubes as air diffuses into the extended gas jets. Ionization waves (IWs) or plasma bullets, which form the jets on the boundaries of an array, encounter higher mole fractions of air earlier compared with the center jet and so are slower or are quenched earlier. The close proximity of the jets produces electrostatic repulsion, which affects the trajectories of the IWs. If the jets are close enough, photoionizing radiation from their neighbors is an additional form of interaction. These interactions are sensitive to the spacing of the jets.

Keywords: plasma jets, ionization waves, plasma medicine, atmospheric-pressure plasmas

(Some figures may appear in colour only in the online journal)

## 1. Introduction

Non-equilibrium atmospheric-pressure plasma jets are one of the primary plasma sources being investigated for use in biotechnology, including the treatment of human tissue—plasma medicine [1–4]. A typical plasma jet consists of a cylindrical tube of a few mm diameter through which a rare gas or a mixture of a rare gas with a small percentage of a reactive gas such as O<sub>2</sub> is flowed [5]. The configuration of the electrodes is varied. At one extreme, the electrodes are two metal bands (one powered, one grounded) on the exterior of the tube, thereby producing a discharge which operates primarily in a dielectric barrier discharge (DBD) mode [6–10]. At the other extreme, a single ring on or a coaxial electrode inside the

tube is powered and the ground is exterior to the tube [11–13]. The voltage is often applied as a sinusoidal or pulse shaped waveform at repetition rates of a few kHz to many tens of kHz. Some variants of plasma jets are powered continuously with radio frequency (rf) power [14, 15] or dc with circuitry to prevent arcing [16]. The surface being treated receives fluxes of radicals and ions delivered by the gas plume emerging from the tube. Mixing of plasma excited species in the gas flowed through the tube with ambient gas (typically air) produces a large variety of such radicals. Gas shrouds which are intended to minimize the mixing between the central plasma excited plume and the ambient air have demonstrated some degree of control of this radical production [17].

High-speed imaging has shown that the plasma plumes emanating from these jets are formed by propagation of

<sup>1</sup> Author to whom any correspondence should be addressed.

ionization waves (IW), often called plasma bullets. The IWs propagate through the tubes and then through the gas phase channel formed by the rare gas injected through the tube into the surrounding air [16, 18]. Plasma jets are often described as *indirect sources*, since if the tube is far enough from the surface, the plasma decays prior to reaching the surface being treated [1]. In practice, the luminous plume from such indirect sources can extend for several cm to actually intersect the surface [8]. Under conditions where the plasma bullet reaches the surface being treated, the term ‘indirect source’ may not be fully descriptive.

For reasons that largely have to do with minimizing gas heating and applied voltages, the diameter of the tube of an individual plasma jet is typically less than a few mm. As a result, an individual jet can only treat small surface areas. In many ways, this is an advantage since small areas (in some cases individual cells) can be treated [19]. In other applications, it may be desirable to treat larger areas. One solution is to group many jets together to form an array [20–22]. Individual ballasted and powered jets enable potentially effective control of jet–jet interactions and plasma–surface interactions. For example, Cao *et al* [20] demonstrated a one-dimensional (1D) array of ten simultaneously ignited jets. Two-dimensional (2D) arrays of spatially confined jets have been demonstrated by Eden and Park [23], Sakai *et al* [24] and Nie *et al* [25]. Ma *et al* have developed arrays of micro-channels embedded in polymer producing micro-jets having a channel diameter of 340  $\mu\text{m}$  and extending almost 4 mm into air [26].

Perhaps an unintended consequence of constructing arrays of plasma jets is that individual plasmas in an array tend to interact with each other [27–33]. For example, densely packed plasma jets in a honeycomb configuration developed by Cao *et al* appeared to have strong jet–jet interaction which produced either divergence or convergence of the plumes of the plasma jets [27]. A similar coupling was observed by J-Y Kim *et al* [28, 29] and S-O Kim *et al* [30] who constructed a seven-jet array (one central jet surrounded by six hexagonally spaced jets). Under select conditions, seven distinct plasma plumes were formed. A mode transition would sometimes occur where the central plasma plume became optically very intense and the outer plumes extended only a short distance beyond the end of their tubes. The intensity of the center plume was significantly greater than when operating as a single jet, suggesting a synergistic reinforcement of the center jet at the expense of the outer jets.

Kim *et al* [30] also investigated the conditions that produced jet-to-jet coupling. They found that the array must have an appropriate gas flow of 1–3.5 slm to interact. When the gas flow was higher than 3.5 slm the plasma jets no longer interacted with each other, but rather transformed into individually well-collimated plasma plumes regardless of the operating voltage. Kim *et al* [30] and Furmanski *et al* [31] increased the number of outer tubes and found that despite an equally distributed gas flow, the outermost tubes did not produce strong individual plasma plumes. Rather, the plasma plumes were drawn into the central plume, which was, in turn, amplified. As a result, the optical intensity from a 19-jet

array was nearly twice that from a conventional single plasma jet. Fan *et al* investigated an array of seven He plasma jets, a hexagonal structure with a center jet [32]. They observed repulsion of the jets, an effect they attributed to electrostatic repulsion between the jets. These interactions lessened with increased gas flow. Ghasemi *et al* [33] investigated arrays of 2–4 plasma jets and observed significant divergence of the plumes. They attributed this divergence in part to electrostatic repulsion, which through ion momentum transfer also produced divergence of the gas channel.

The dynamics of single plasma jets have recently been computationally investigated. Brok *et al* [34] and Sakiyama and Graves [35–37] modeled an rf powered plasma needle. Sakiyama demonstrated two modes of operation—for low and high plasma powers—and the influence of the gas flow on the discharge structure [37]. They proposed that increasing the gas flow (in a laminar regime) decreases the rate of entrainment of ambient  $\text{N}_2$  into the discharge region. As a result, the Penning ionization of  $\text{N}_2$  by He excited states produced in the discharge occurs dominantly in an off-axis annular region. Naidis [38–40] addressed the behavior of positive and negative plasma bullet propagation along a helium channel in ambient air, obtaining the ring-shaped structures typically observed experimentally. Using a prescribed density of He and air, Boeuf *et al* showed that the plasma jet is similar to a streamer guided by a helium channel [41]. Employing a coupled model of fluid dynamics and plasma transport of He flow into air, Raja and co-workers found that ionization is wall-hugging inside the dielectric channel and centered in the He channel downstream [42]. They also found that Penning ionization, though important, does not dominantly sustain the IW compared with electron impact ionization of the infusing air.

In this paper, we build upon these prior findings and discuss results from a computational investigation of the properties of small arrays of micro-plasma jets. In the following discussion with a single jet as a baseline, we consider two- and three-jet arrays having variable spacing. A He/ $\text{O}_2$  mixture is flowed through the tubes of the jets into ambient humid air. We show that jet–jet interactions primarily depend on how densely the tubes are packed and on their number. With a large separation between tubes, individual helium channels in the air are formed by the plumes emanating from the tubes. These plumes individually dissipate by the He and air inter-diffusing. IWs in the form of plasma bullets then propagate through the individual He channels as separate entities until the IWs die. By dying, we mean that the local  $E/N$  (electric field/gas number density) is below that required to further sustain the IW. The self-sustaining  $E/N$  is larger in locations where the mole fraction of air is larger. The He plumes from tubes that are densely packed tend to merge into one single stream before dissipating. Plasma bullets from two tubes, though electrostatically repelling, are confined within the merged He plumes where the  $E/N$  is above the self-sustaining values. The two IWs following the boundaries of the He channels merge into a single plasma bullet. The physics is similar for three tube arrays where the three bullets propagate within a single helium stream. The central bullet of the array

becomes the strongest, whereas the two surrounding bullets are electrostatically pushed to the channel boundaries and decay with time.

The model used in this investigation is briefly described in section 2. The main features of a single jet are discussed in section 3. Arrays of two and three jets with different tube separations are discussed in sections 4 and 5. Our concluding remarks are in section 6.

## 2. Description of the model

This investigation of jet–jet interactions was conducted using the modeling platform *nonPDPSIM*. A 2D simulator, *nonPDPSIM*, solves transport equations for charged and neutral species, Poisson’s equation for the electric potential, the electron energy conservation equation for the electron temperature and Navier–Stokes (NS) equations for the neutral gas flow. The model is essentially the same as used in [43, 44].

The computation begins by injecting a He/O<sub>2</sub> mixture through the tube(s) into ambient humid air. During this part of the computation only the neutral flow NS equations and individual transport equations for neutral species are integrated. These equations for individual species are integrated in lock-step with the NS equations until the steady state is reached. By lock-step we mean that the NS and neutral transport equations are integrated in parallel using the same time steps.

The flow conditions are laminar, essentially incompressible and isobaric. However, the injection of He into air produces severe gradients in the mass density and in mole fractions of the gas species while the gradient in total number density of the gas may be small. Therefore, a modified form of the NS equations was solved in which we include continuity equations for the total gas density and volumetric heat capacity. With knowledge of the mole fractions of the individual gas species from their respective continuity equations, we can continually correct the total mass density that is required elsewhere in the NS equations.

Once the neutral flow is time integrated to the steady state, the plasma transport equations and Poisson’s equations are turned on and the voltage on the electrode is pulsed. At this time, a time-slicing or a sub-cycling technique is used. The time step for integration of the plasma transport, electron energy, neutral species continuity equations and Poisson’s equation is  $\approx 10^{-10}$  s, which is much smaller than that required for solution of the NS equations. We therefore integrate the plasma transport equations for 1–2 ns while holding the flow speeds constant, followed by an integration of the NS equations for the same time while holding the plasma properties constant. The combined plasma transport and neutral flow equations are integrated in this fashion until the IW terminates and the plasma decays. At that time, any remaining densities of charged particles are set to zero, the plasma transport and Poisson’s equation are no longer integrated and only the neutral flow and chemistry equations are integrated using appropriately longer time steps.

Schematics of the model geometry for plasma jets are shown in figure 1. An individual plasma jet consists of a glass

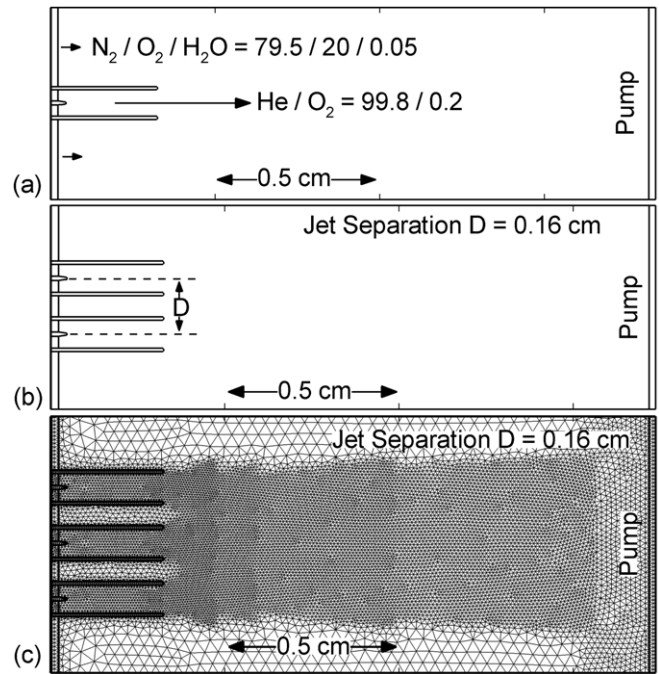


**Figure 1.** Geometry used for simulation of (a) one-, (b) two- and (c) three-jet arrays. High-voltage pulses are applied to pin electrodes. The opposite plane is a grounded electrode which also serves as a pump port. The separations between the centers of the tubes are  $D = 0.32, 0.16$  and  $0.105$  cm. A He/O<sub>2</sub> = 99.8/0.2 mixture is injected through each of the tubes at a flow rate of 5 lpm. Humid air is flowed parallel to the tubes. The computational domain is covered by unstructured meshes with several refinement zones to resolve the path of the ionization wave, as shown in the bottom frame.

tube ( $\epsilon/\epsilon_0 = 3$ ) with an inner diameter of 0.08 cm and an outer diameter of 0.1 cm. The separations between the center of the tubes are  $D = 0.32$  cm, 0.16 cm and 0.105 cm for large, medium and small separations, respectively. High-voltage pulses of  $-17$  kV (for a single jet) and  $-28$  kV (for two- and three-jet arrays) with a rise time of 15 ns are simultaneously applied to pin metal electrodes ( $50 \mu\text{m}$  radius of curvature) centered inside the tubes. The voltage is then held constant for the duration of the current pulse. The different voltages were used so that the average electric field across the jets would be approximately the same. A second grounded metal electrode is placed up to 1.8 cm downstream from the nozzle which is also used as the pump for the jet flow. Since the model is 2D, we approximate arrays of circular tubes as stacks of slots. The unstructured mesh consists of triangles with several refinement zones to resolve the regions where the plasma density is high and IWs propagate. The unstructured meshes consisted of up to 13 000 nodes for three-jet arrays. The IWs were initiated by small clouds of seed electrons and O<sub>2</sub><sup>+</sup> ions placed near the pin electrodes in each tube. The clouds have Gaussian profiles  $300 \mu\text{m}$  with a peak density of  $5 \times 10^{11} \text{ cm}^{-3}$ . The IWs are then naturally sustained by their own space charge driven electric field as in conventional streamers.

This particular initial seed was chosen for convenience. Provided the spatial extent of the initial seed is sufficiently small, the final outcome is insensitive to the magnitude of the initial seed and only affects the induction time between

application of the voltage and launching of the IW inside the tube. (Smaller seeds have longer induction times.) These trends were confirmed by varying the peak value of the initial seed from  $5 \times 10^8$  to  $5 \times 10^{11} \text{ cm}^{-3}$ . No significant change in the final results was observed.

The voltages we have used are somewhat higher than typically used in experiments. This is in large part a consequence of our computing only a single pulse that propagates into a non-ionized gas. In experiments at high repetition rates (10 kHz), the residual electron density prior to the next pulse can be as large as  $10^{10} \text{ cm}^{-3}$  or there is a large density of  $\text{O}_2^-$  which provides a low threshold energy source of electrons by electron impact or photo-detachment. Both of these effects serve to lower the operating voltage. In many models [40], a uniform background density of electrons is used, as high as  $10^{10} \text{ cm}^{-3}$ , to account for prior pulses and to provide a pre-ionized channel for jet propagation. We have chosen to have the jets propagate into non-ionized gas, and so voltages are naturally higher.

An atmospheric-pressure  $\text{He}/\text{O}_2 = 99.8/0.2$  mixture was flowed through each of the tubes at 5 slm into humid room air ( $\text{N}_2/\text{O}_2/\text{H}_2\text{O} = 79.5/20/0.5$ ). In order to minimize vortices and shear layers between the jets and the ambient gas, the room air is also flowed between the tubes collinearly to the jets as shrouds. This results in smooth zones of air diffusing into the jets of  $\text{He}/\text{O}_2$  and vice versa. The air flowed between the tubes is a requirement of the 2D calculation. In the absence of the air flowed between the tubes, the He jets would, in the steady state, immediately merge since there would otherwise be no mechanism for air to penetrate into the interior sides of the jets. The  $\text{He}/\text{O}_2$  mixture was chosen to align with experimental observations that this fraction of  $\text{O}_2$  in He produces the highest uniformity and optical emission [25].

The chemical reaction mechanism includes electrons; 34 other species and more than 200 reactions. The species in the model are e, He,  $\text{He}(2^1\text{S})$ ,  $\text{He}(2^3\text{S})$ ,  $\text{He}(2^1\text{P})$ ,  $\text{He}(2^3\text{P})$ ,  $\text{He}(3\text{S})$ ,  $\text{He}(3\text{P})$ ,  $\text{He}_2^*$ ,  $\text{He}^+$ ,  $\text{He}_2^+$ ,  $\text{N}_2$ ,  $\text{N}_2^*$  ( $A^3\Sigma$ ,  $B^3\Pi$ , higher),  $\text{N}_2^{**}$  ( $C^3\Pi$ , higher),  $\text{N}_2^+$ , N,  $\text{N}_4^+$ ,  $\text{O}_2$ ,  $\text{O}_2(1\Delta)$ ,  $\text{O}_2(1\Sigma)$ ,  $\text{O}_2^+$ ,  $\text{O}_2^-$ ,  $\text{O}(1\text{D})$ ,  $\text{O}^-$ ,  $\text{O}_3$ , NO,  $\text{NO}^+$ ,  $\text{NO}_2$ ,  $\text{H}_2\text{O}$ ,  $\text{H}_2\text{O}^+$ ,  $\text{H}_2$ , H, OH and  $\text{HO}_2$ . The reaction mechanism consists of a subset of the reactions discussed in [45–47], which involve these species. This is a reduced reaction mechanism compared with those used in global models [48], a situation which is necessitated by the additional computational burden of the 2D calculation. Although vibrational states of  $\text{N}_2$  and  $\text{O}_2$  are not explicitly followed as separate species, electron impact energy loss processes with the ground state species for vibrational excitation are included in the solution of Boltzmann's equation for rate coefficients. We have assumed that photoionization occurs dominantly from resonance radiation from  $\text{He}(2^1\text{P})$  (which can be heavily trapped) which is absorbed by  $\text{O}_2$ .

The phenomena we are addressing, for example bundles of plasma jets, clearly have three-dimensional (3D) characteristics, whereas our approach has used 2D modeling using the Cartesian coordinates. There are likely important differences between the 2D and 3D approaches. Perhaps the most important here is a possible over-representation of the electrostatic interference between adjacent plasma jets. In 3D

calculations, the curvature of the streamer head typically has a smaller radius of curvature compared with the 2D Cartesian analog. This results in there being a larger electric field at the head of the streamer in 3D (or in 2D cylindrically symmetric coordinates) and a more rapid fall-off of potential (and so smaller electric field) as a function of distance compared with 2D. As a result, the 2D approximation may underestimate the rate of avalanche in the streamer head and overestimate the effects of streamer interactions based on electrostatic coupling.

### 3. Single jet dynamics

High-speed imaging has shown that the luminous plume of plasma jets typically results from bullet-like structures traveling with speeds up to  $10^8 \text{ cm s}^{-1}$  [40]. These plasma bullets are essentially IWs or streamers. They differ from conventional IWs or streamers propagating in a uniform gas due to their confinement either by the physical boundaries of the glass tube or by the chemical boundaries produced by, for example, a helium plume extending into air.

The optical emission and predicted distribution of plasma from many such plasma jets are often annular. Within the tube, this annular structure is likely due to electric field enhancement at the gas–dielectric interface. In the gas phase, the annular structure is in part due to the interaction of the plasma-generated excited states and ions within the plume, typically He, with the gas surrounding the plume, typically air. For He jets into air, there is a finite distance of propagation of the plasma bullet, which is in part due to the fluid dynamics of the plasma jet. Since  $\text{N}_2$  and  $\text{O}_2$  have a higher self-sustaining  $E/N$  than helium (or He doped with small amounts of  $\text{O}_2$ ), an IW which propagates through a He plume will terminate as the air mole fraction increases within the plume due to mixing with the ambient gas. Although there are Penning reactions of  $\text{N}_2$  and  $\text{O}_2$  by He excited states and photoionization of the air originating from helium excited states, these reactions are typically not able to offset the increasing self-sustaining  $E/N$  produced by the infusing air. As a result, the IW dies.

The steady-state densities of He,  $\text{N}_2$  and  $\text{O}_2$  in the absence of a plasma are shown in figure 2 for  $\text{He}/\text{O}_2$  injected through a single tube into flowing humid air. Profiles of these densities 0.2 cm from the exit of the nozzle are shown in figure 2(d). At this distance, advection by helium produces a helium-dominated profile. Although close to the nozzle, there is some finite diffusion of  $\text{N}_2$  to the axis (mole fraction 0.02). The on-axis mole fraction of He decreases to 60% at a distance 1 cm downstream of the nozzle.

Computationally, after the steady-state gas flow is established, a voltage pulse of  $-17 \text{ kV}$  is applied to the pin electrode to initiate the discharge. Time sequences (timings are relative to the onset of voltage) of electron density (left column) and electron impact ionization source (right column) are shown in figure 3(a). The maximum electron density within the tube is a few  $10^{12} \text{ cm}^{-3}$  and the electron impact ionization source is a few  $10^{20} \text{ cm}^{-3} \text{ s}^{-1}$ . Other than maximum near the tip of the electrode, both are annular inside the tube due to electric field enhancement at the interface of the gas and the dielectric tube. This annular nature extends for 0.2 cm beyond

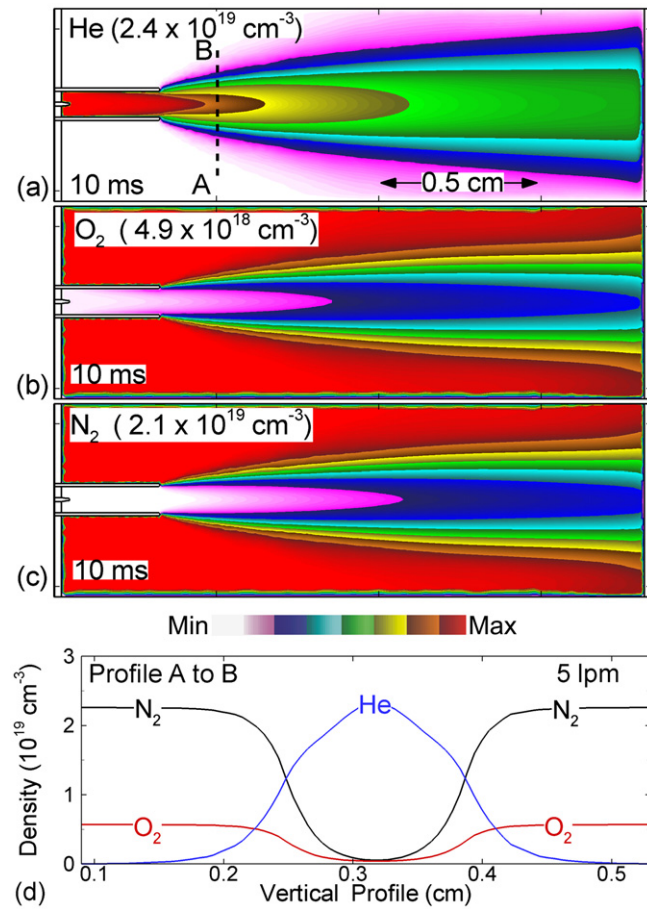


**Figure 2.** Steady-state flow for a single jet before the application of the voltage pulse. Images show the densities of (a) helium, (b) oxygen and (c) nitrogen flow patterns. (d) Vertical profile of densities along the A–B chord at a distance of 0.2 cm from the nozzle. The contours are plotted on a linear scale with the maximum value shown in each frame.

the end of the tube before transitioning to a center peaked profile. For these conditions, the bullet dies 0.7 cm beyond the end of the tube where the mole fraction of air exceeds 60%. The rapid decay of electron density results from attachment to  $O_2$  and the increase in the self-sustaining  $E/N$  that results from the infusion of air. For example, the maximum  $E/N$  in the head of the IW as the wave emerges from the tube is 98 Td ( $1 \text{ Td} = 10^{-17} \text{ V cm}^2$ ) where the He mole fraction is 99% but is below self-sustaining for an air mole fraction of 60%.

Vertical profiles of electron, NO and O atom densities are shown in figure 3(b) at a point 0.1 cm beyond the end of the tube. Since we simulate only a single pulse here, the gas temperature does not increase more than a few degrees above ambient. The profiles are annular as observed in experiments [37, 49] in which the shapes are attributed to Penning ionization between helium metastable states and air. In our simulations the annular shape of the electron density is partly attributable to these Penning processes. However, the electron density is annular within the tube where Penning processes are not important and this shape persists downstream. The NO density is most annular which reflects the diffusion of  $N_2$  into the He plume. The O density is least annular as production of O atoms is dominated by electron impact dissociation of the

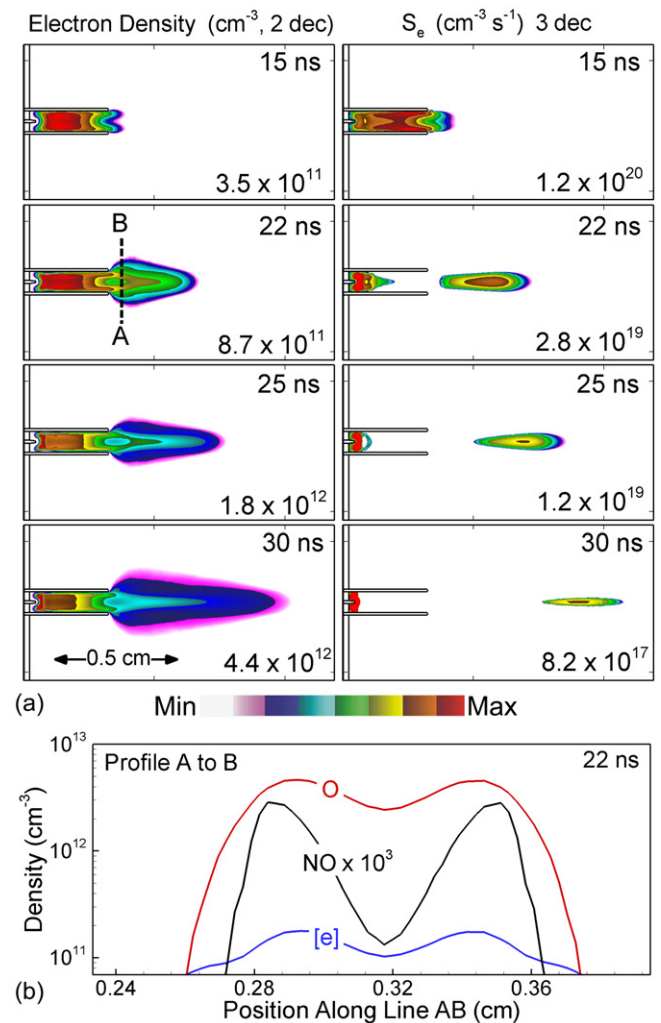


**Figure 3.** Time sequence of (a) electron impact ionization source,  $S_e$  (right column) and electron density (left column). (b) Densities of O, NO and electrons at 22 ns along the chord A–B. The applied voltage is  $-17 \text{ kV}$ . Time indicated in each frame is relative to application of the voltage.  $S_e$  indicates the position of the IW that would be perceived as a luminous front or a bullet in the experiments. The plasma bullet decays approximately in the middle of the gap where the mole fraction of air exceeds 60%. The contours are plotted on a log scale over two decades with the maximum value shown in each frame.

$O_2$  within the injected gas. These findings generally agree with experimental and computational results of Karakas *et al* [50] and Xiong *et al* [51]. They found that when the He mole fraction in the plume fell below 0.45–0.5 (depending on conditions) the plasma bullet no longer propagated.

The radicals produced by plasma jets that are of interest to biomedical applications include reactive nitrogen species (RNS), which result from reactions between the plasma-activated species in the core of the He jet and air diffusing into the jet. For example, the predicted NO density for a single discharge pulse is shown in figure 4 during the time that the plasma is active (0–50 ns) and during the afterglow when the plasma is extinguished. (The line contours indicate the mole fraction of air.) For our conditions (near ambient gas temperature) the production of NO is dominated by the reaction  $N + O_2 \rightarrow NO + O$  having a rate coefficient

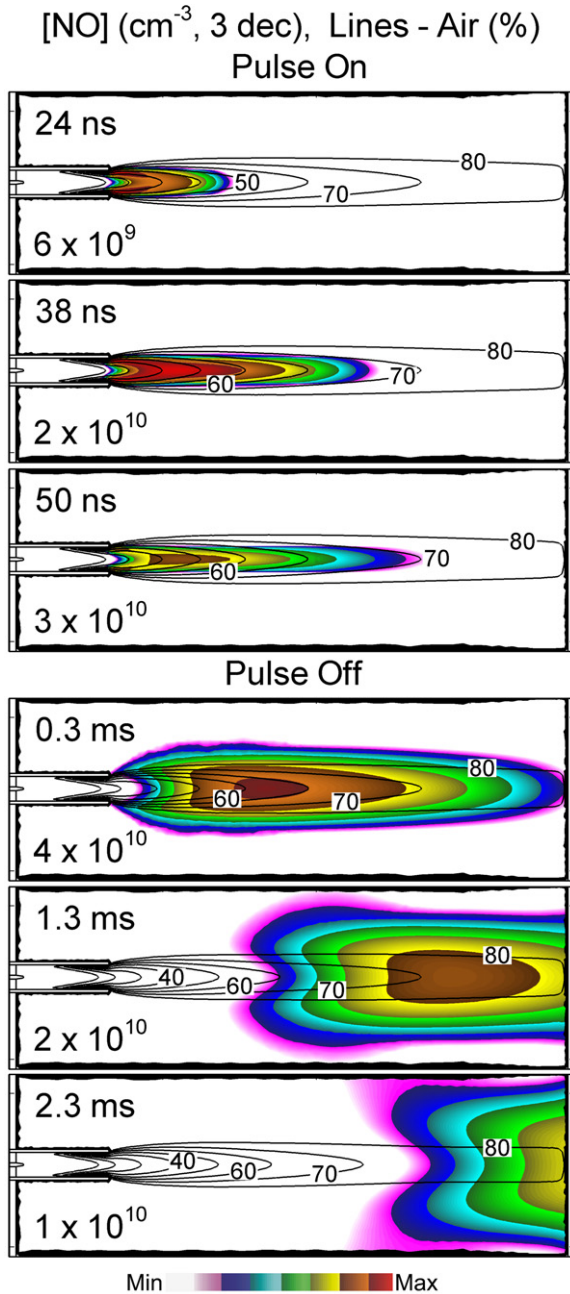


**Figure 4.** Time evolution of NO density for a single jet (top) during a short voltage pulse of 50 ns and (bottom) during 2.3 ms of flow after the voltage pulse. The NO density is shown on a three-decade log scale with the maximum value shown in each frame. The contours are labeled with the mole fraction of air. NO is initially produced in a narrow cylindrical channel near the tube. After the pulse the NO cloud detaches from the tube and convects downstream.

of  $8 \times 10^{-17} \text{ cm}^{-3} \text{ s}^{-1}$ . N atoms are produced dominantly by electron impact dissociation of  $\text{N}_2$  first in an annular region near the edge of the tube and downstream on the axis. The secondary sources of N atoms include dissociative recombination of  $\text{N}_2^+$  and dissociative Penning reactions with He excited states. The shift of the N atom production to on axis is a consequence of the plasma shifting from annular to on axis, and the increasing mole fraction of  $\text{N}_2$  on axis. After the

IW decays (40–50 ns) the production of N atoms by electron impact dissociation essentially stops, with there being minor continued production by dissociative recombination. At this point, the maximum NO density is  $3 \times 10^{10} \text{ cm}^{-3}$ . Since the rate coefficient for NO production is small, the N atoms persist for many milliseconds and continue to produce NO at a slow rate during the afterglow. At this juncture, the NO simply advects downstream with the bulk gas flow, with a spatial distribution that widens due to diffusion. This advecting structure could be thought of as a radical bullet, in analogy to the plasma bullet. For pulse repetition frequencies of tens of kHz, the radical bullets will overlap to form a continuous plume of NO. For pulse repetition frequencies of a few kHz or less, the radical bullets may remain distinct.

#### 4. Two-jet arrays

The experimentally observed interactions between multiple jets may result from electrostatic, photolytic and gas dynamic origins. The electrostatic interactions result from there being a net charge density in the head of atmospheric-pressure IWs. The net charge density is in part the source of the large  $E/N$  in the head of the IW that sustains avalanche. The net charge densities of adjacent streamers of the same polarity will exert forces on the other. The photolytic interactions result from ionizing radiation produced by the adjacent streamer. Finally, the gas dynamic interactions result from the merging of flow fields of closely spaced jets producing gas mole fractions very different from a single isolated jet.

The He densities for two-jet arrays having large (0.32 cm), medium (0.16 cm) and small (0.105 cm) spacing are shown in figure 5. The vertical profiles 2 mm downstream of the nozzle are also shown. For jets that are sufficiently separated, the He channels formed by each jet remain distinct downstream. As the spacing between the jets diminishes, the He plumes begin to merge, resulting in a single, albeit initially wider, He flow channel. This merging of the channels will occur later with a higher flow rate and larger separation but will, in principle, eventually occur. We acknowledge that this effect is likely exaggerated by the 2D nature of the calculation. In three dimensions, air diffuses into the He plumes from around the entire periphery of the jets and so it is more likely that the individual jets will individually dissipate (as in figure 2) prior to merging (as shown in figure 5).

Plasma characteristics (electron impact ionization source, electron density, negative space charge and photoionization source) for two plasma jets having a large separation ( $D = 3.2 \text{ mm}$ ) are shown in figure 6. With this separation and with synchronized voltage pulses, two IWs or plasma bullets propagate through each individual helium channel with two distinct electron impact ionization sources ( $4.2 \times 10^{21} \text{ cm}^{-3} \text{ s}^{-1}$  at 26 ns), as shown in figure 6(a). The IWs propagate with the same speed ( $8 \times 10^7 \text{ cm s}^{-1}$ ) and the same electron density ( $(7-8) \times 10^{11} \text{ cm}^{-3}$  in the tube and  $3 \times 10^{12}$  to  $1 \times 10^{13} \text{ cm}^{-3}$  in the plume 0.7 cm from the tube at 26 ns), as shown in figure 6(b). Note that there is a halo of electron density at the edges of both tubes having a local maximum density of  $7 \times 10^{11} \text{ cm}^{-3}$ . These halos are the result of

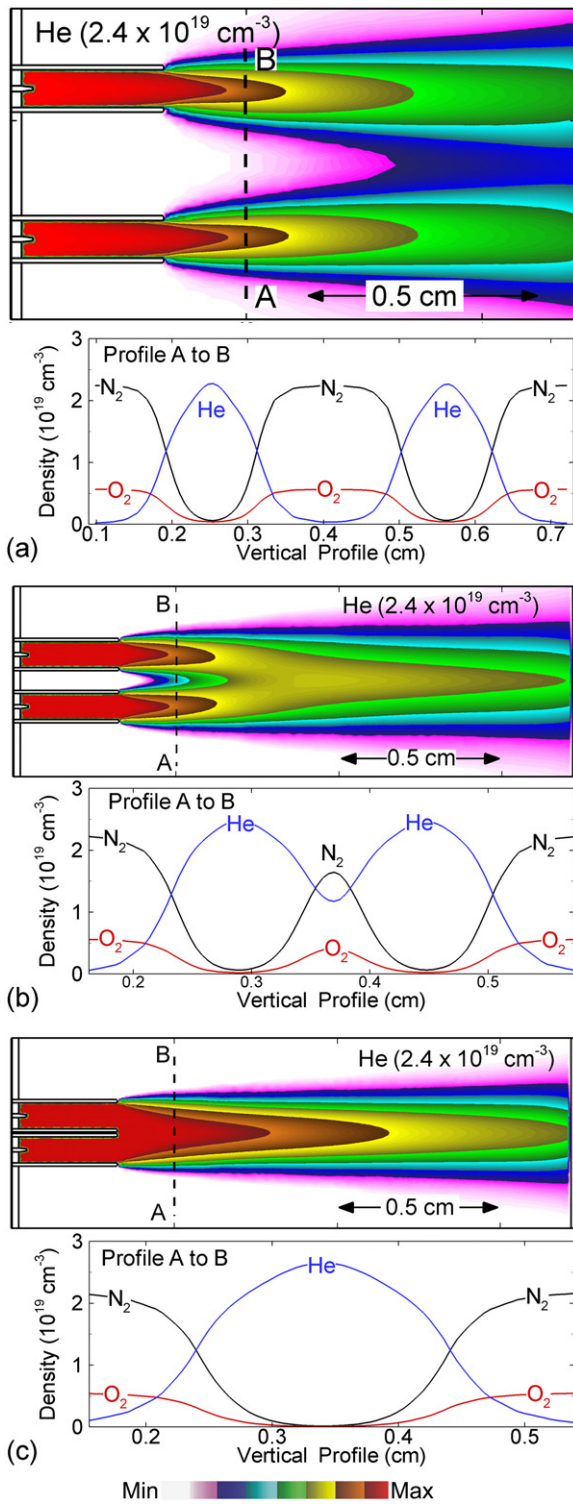


**Figure 5.** Steady-state flow for a two-jet array before the application of the voltage pulse. Images show the densities of helium and vertical profiles of He, N<sub>2</sub> and O<sub>2</sub> for (a) large (0.32 cm), (b) medium (0.16 cm) and (c) small (0.105 cm) separation between the tubes. The vertical profiles are shown along the A–B chord at a distance of 0.2 cm from the nozzles. The contours are plotted on a linear scale with the maximum value shown in each frame. For large separations, distinct helium channels are produced. For closely spaced tubes the helium channels merge into a single stream.

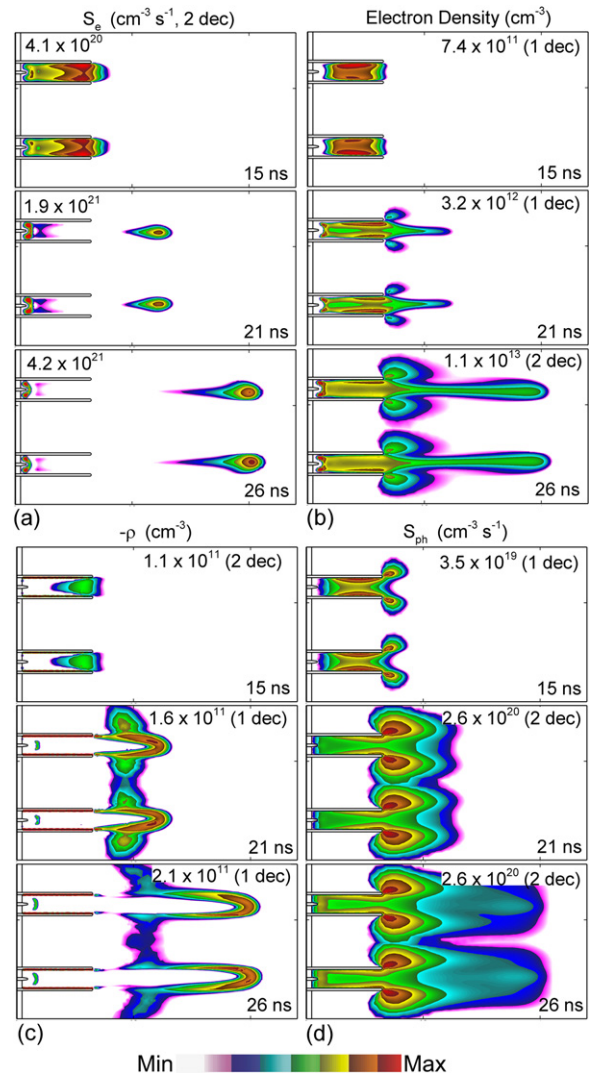


**Figure 6.** Plasma characteristics for a two-jet array with a large separation ( $D = 0.32$  cm) for times after the voltage is applied. (a) Electron impact ionization source, (b) electron density, (c) negative space charge and (d) photoionization source. With synchronized voltage pulses two bullets, though repelling, propagate through each individual helium channel. Negative space charge outlines the contours of each IWs. The contours are plotted on a log scale with the maximum value shown in each frame.

photoionization (figure 6(d)) by the VUV emission from He resonance states. The photoionization source is particularly intense in the halo (maximum value  $2.6 \times 10^{20} \text{ cm}^{-3} \text{ s}^{-1}$  at 26 ns) as at this location the He excited state density is still high ( $1.5 \times 10^{11} \text{ cm}^{-3}$ ) and within a few absorption lengths of a high density of O<sub>2</sub>. These halos have also been seen in optical emission in arrays of micro-jets [28–31].

The two plasma jets are not identical—they have a mirrored asymmetry that results from their mutual Coulomb repulsion. Since the jets are both negative discharges, the IWs have a net negative charge that outlines the region of high  $E/N$  in the avalanche front, as shown in figure 6(c). This net negative space charge, exceeding  $10^{-8} \text{ C cm}^{-3}$ , produces enough electrostatic potential to force the plasma inside the tubes to opposite walls (figure 6(b)) and to skew the electron impact ionization sources to opposite walls inside the tubes.

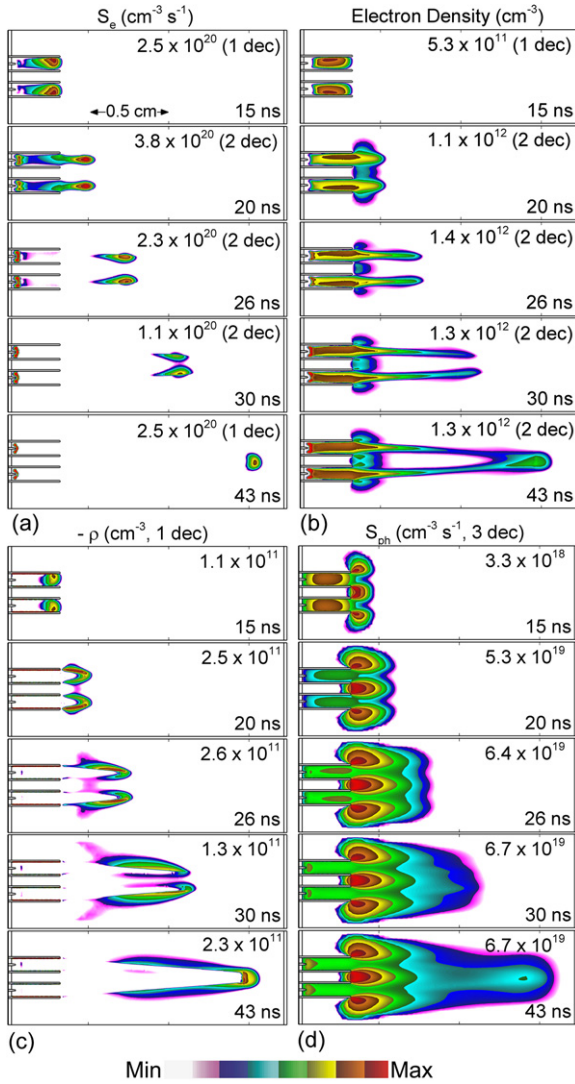


**Figure 7.** Plasma characteristics for a two-jet array with a medium separation ( $D = 0.16$  cm) for times after the voltage is applied. (a) Electron impact ionization source, (b) electron density, (c) negative space charge and (d) photoionization source. With smaller separation there is more noticeable electrostatic repulsion of the bullets inside the tubes. Although repelling, two distinct bullets initially propagate. The merging of the helium channels at a further distance results in merging of the bullets. The contours are plotted on a log scale with the maximum value shown in each frame.

Outside the tube in the plumes, the ionization sources are limited by being electrostatically pushed off axis into regions where the air mole fraction is larger and so the self-sustaining  $E/N$  is larger.

Plasma characteristics (electron impact ionization source, electron density, negative space charge and photoionization) for two plasma jets with medium separation ( $D = 1.6$  mm) are shown in figure 7. Qualitatively, inside and immediately downstream of the tube, the plasma properties appear the same as for the larger separation. As with the wider spacing, the plasma bullets and the resulting plume of electron density ( $5.3 \times 10^{11} \text{ cm}^{-3}$  in the tube and  $1.3 \times 10^{12} \text{ cm}^{-3}$  in the plume 0.7 cm from the tube at 30 ns) are in distinct channels. However, with this smaller separation there is more noticeable

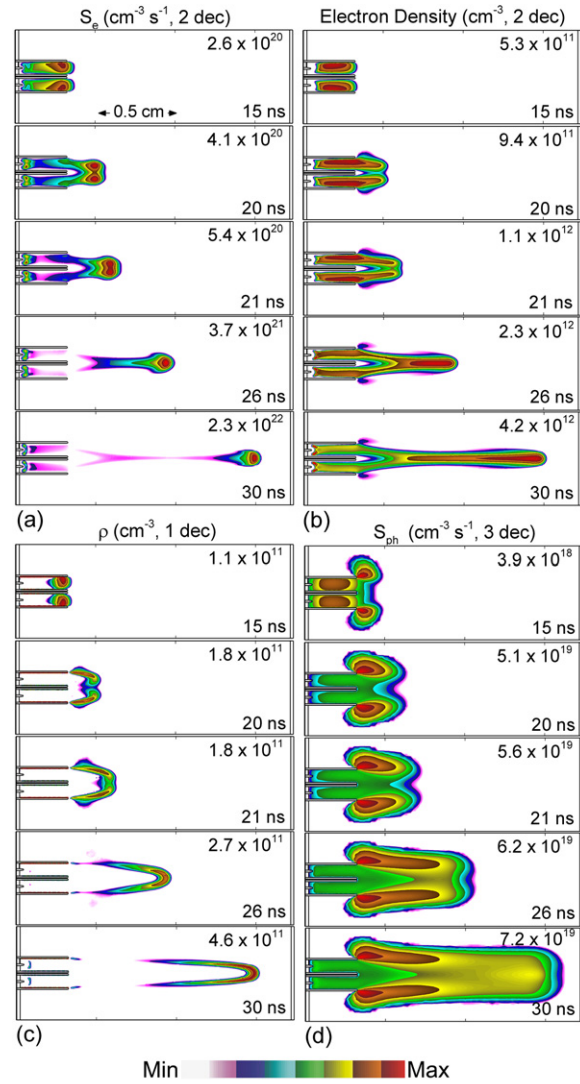


**Figure 8.** Plasma characteristics for a two-jet array with a small separation ( $D = 0.105$  cm) for times after the voltage is applied. (a) Electron impact ionization source, (b) electron density, (c) negative space charge and (d) photoionization source. Severe electrostatic repulsion of the bullets inside the tubes occurs. Due to the rapidly merged helium channels, two bullets from each tube must propagate inside the single helium channel, electrostatically forced to the air boundaries until the IWs merge. The contours are plotted on a log scale with the maximum value shown in each frame.

electrostatic repulsion between the two IWs, particularly inside the tubes. When the IWs emerge from the tubes, the electrostatic repulsion is so large that the ionization sources are pushed against the He–air boundary. The plasma plumes are now close enough that the halos of electron density produced by photoionization overlap.

The IWs initially propagate within their own He channels. However, the helium channels eventually merge downstream which produces a merging of the IWs. The IWs appear to curve inward as they follow the contour of approximately 0.6–0.7 He mole fraction. As a result of the merging of the IWs, there is no longer electrostatic repulsion pushing the separate IWs into the regions of lower He mole fraction. The plasma bullet is then

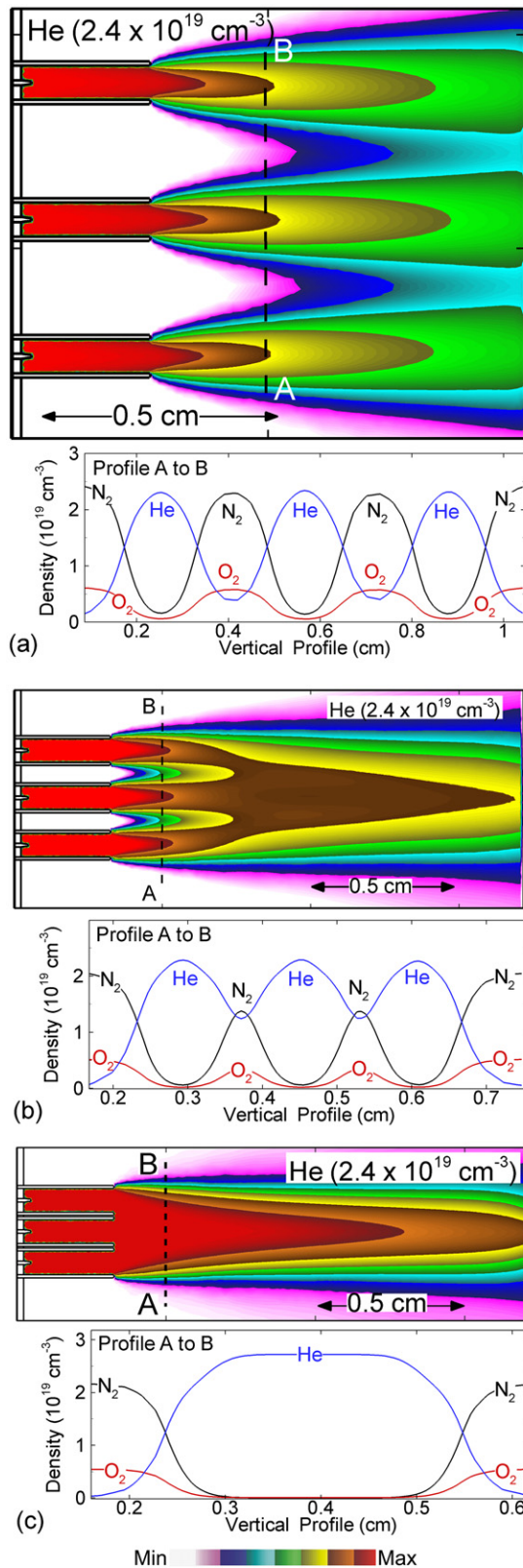


**Figure 9.** Steady-state flow for a three-jet array before the application of the voltage pulse. Images show the densities of helium and vertical profiles of He, N<sub>2</sub> and O<sub>2</sub> for (a) large (0.32 cm), (b) medium (0.16 cm) and (c) small (0.105 cm) separation between the tubes. The vertical profiles are shown along the A–B chord at a distance of 0.2 cm from the nozzles. The contours are plotted on a linear scale with the maximum value shown in each frame.

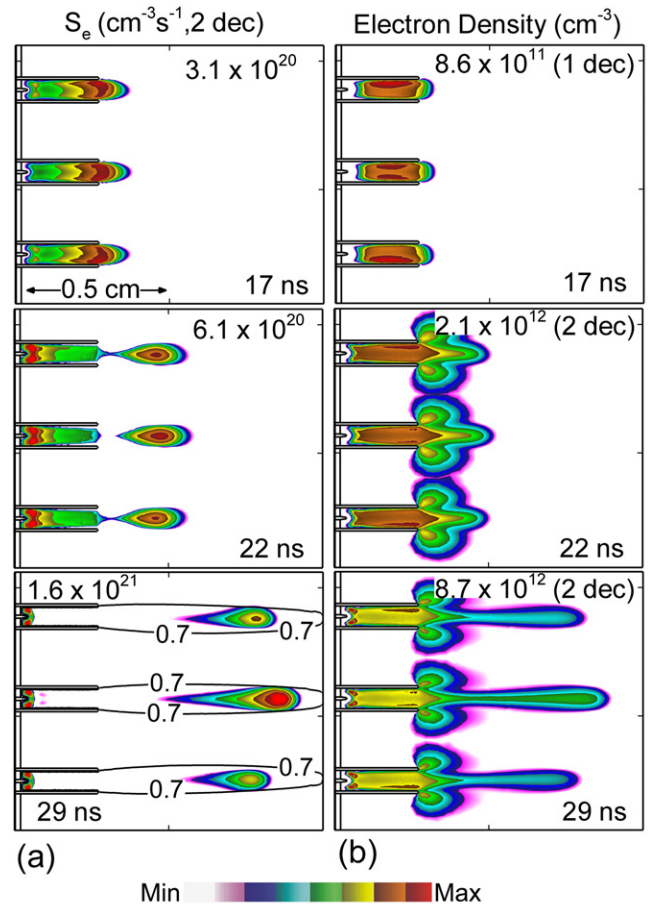


**Figure 10.** Plasma characteristics for a three-jet array with a large separation ( $D = 0.32$  cm) for times after the voltage is applied. (a) Electron impact ionization source and (b) electron density. The contours are plotted on a log scale with the maximum value shown in each frame. The lines show the contour of 70% helium mole fraction. The top and bottom IWs are electrostatically pushed into regions of lower He mole fraction, thereby slowing with a lower density than the center IW.

centered in the He channel and increases its peak intensity, as indicated by the ionization source.

The propagation of parallel IWs is an intrinsically unstable configuration. By that we mean that two IWs propagating parallel to each other will not remain identical in their properties under the influence of any small perturbation. This instability results from the fact that each IW produces a conductive channel that shorts out the electric potential in its wake. This increase in conductivity affects adjacent IWs by reducing the electric field in their vicinity. If due to some small perturbation one IW is slightly ahead of its neighbor, the propagation speed of the neighbor will decrease while that of the forward IW increases. This effect can be seen in the electron density in figure 7(a) where the perturbation is caused by very small asymmetries in the unstructured mesh. This intrinsic instability has been quantified in the context of fingering of ionization fronts [52].

The IWs for two closely spaced plasma jets (with a separation of  $D = 0.105$  cm) are more severely affected by their neighbor. Plasma characteristics for the closely spaced jets are shown in figure 8. First, the closer proximity produces

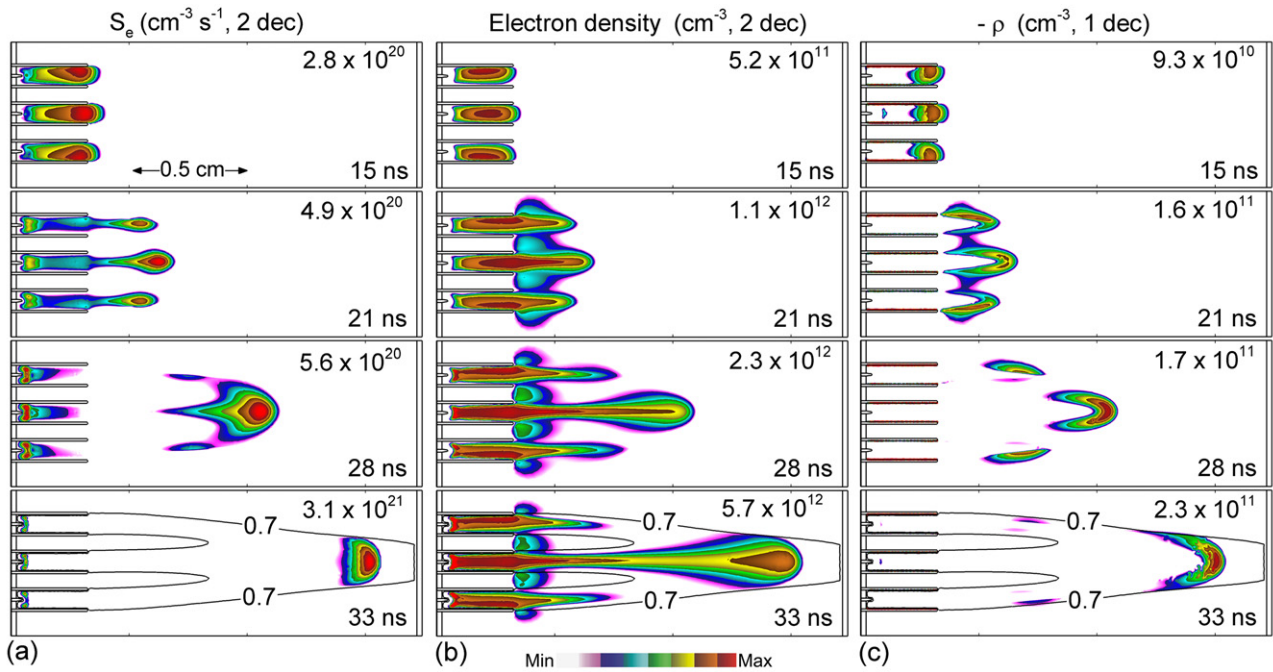


**Figure 11.** Plasma characteristics for a three-jet array with a medium separation ( $D = 0.16$  cm) for times after the voltage is applied. (a) Electron impact ionization source, (b) electron density and (c) negative space charge. The contours are plotted on a log scale with the maximum value shown in each frame. The lines show the contour of 70% helium mole fraction. With more rapid merging of the He channels, the top and bottom IWs are electrostatically pushed into regions of lower He mole fraction and die before merging with the center IW.

even more severe electrostatic repulsion of the IWs at all locations and particularly inside the tubes. The electron density and ionization source inside the tubes have maxima on opposite walls. The electron density decreases by a factor of five to seven from the far side to the near side due to this repulsion. For these conditions, the He plumes merge nearly immediately upon exiting the tubes. In spite of the merged He plumes, the electrostatic forces between the IWs with this small spacing are sufficient to push the ionization sources to the outer boundaries of the merged channel. The IWs continue to propagate as distinct plasma bullets for a short distance (3–4 mm), albeit at the edges of the converging He channel. When the IWs are in the tubes the gas is a homogeneous mixture of He with a trace of  $O_2$ —the dominant force that determines their axial locations is the electrostatic repulsion, and so the maxima in  $n_e$  and  $S_e$  are on opposite walls. When the IWs emerge from the tubes, they propagate into the He channel that is progressively narrowing as the two He channels merge and air diffuses into the He channels. The bullets, are confined within the boundaries of the common narrowing helium channel, outside of which the air-rich regions have a higher self-sustaining  $E/N$ . Despite the electrostatic repulsion between the IWs, the two plasma plumes eventually fully merge into a single IW.

When comparing plasma characteristics between different cases, it is more appropriate to compare, for example, the electron densities when the IWs are approximately at the same location rather than at the same time since initiation. Ionization rate coefficients which determine the speed of propagation are sensitive to the local  $E/N$  and gas mixture which in turn are sensitive to the proximity of other streamers. So depending on

the spacing and number of co-propagating jets, there may be time delays in initiating the IWs from one case to another.

### 5. Three-jet arrays

The steady-state gas flows for He emerging into air and He–air profiles 2 mm downstream from the tubes for three-jet arrays are shown in figure 9. For a separation of 3.2 mm, the jets form three distinct helium channels. For the 1.6 mm separation, the He channels are initially distinct but ultimately merge. For the smallest separation, the He channels merge within a diameter of the tube openings.

The electron density and electron impact ionization source for a three-jet array are shown in figure 10 for the largest separation. With this separation and with synchronized voltage pulses, three plasma bullets propagate through their individual helium channels. However, even at this separation, there is significant electrostatic repulsion. Inside the tubes, the electron density ( $9 \times 10^{11} \text{ cm}^{-3}$  at 17 ns) and ionization sources ( $3 \times 10^{20} \text{ cm}^{-3} \text{ s}^{-1}$  at 17 ns) of the top and bottom jets are pushed against their outer walls. The change in electron densities for the top and bottom tubes across the tubes is by a factor of 3 to 4. Upon emerging from the tubes, the IWs of the top and bottom jets are pushed towards the outer boundary of the He channel where the air mole fraction is larger. The middle jet is centered within its He channel by the oppositely directed electrostatic forces from the top and bottom channels. (This is best illustrated by the ionization sources at 29 ns.) The end result is that the top and bottom jets, propagating through a higher mole fraction of air, begin to slow and decay relative to the middle bullet. Although the plasma bullets electrostatically

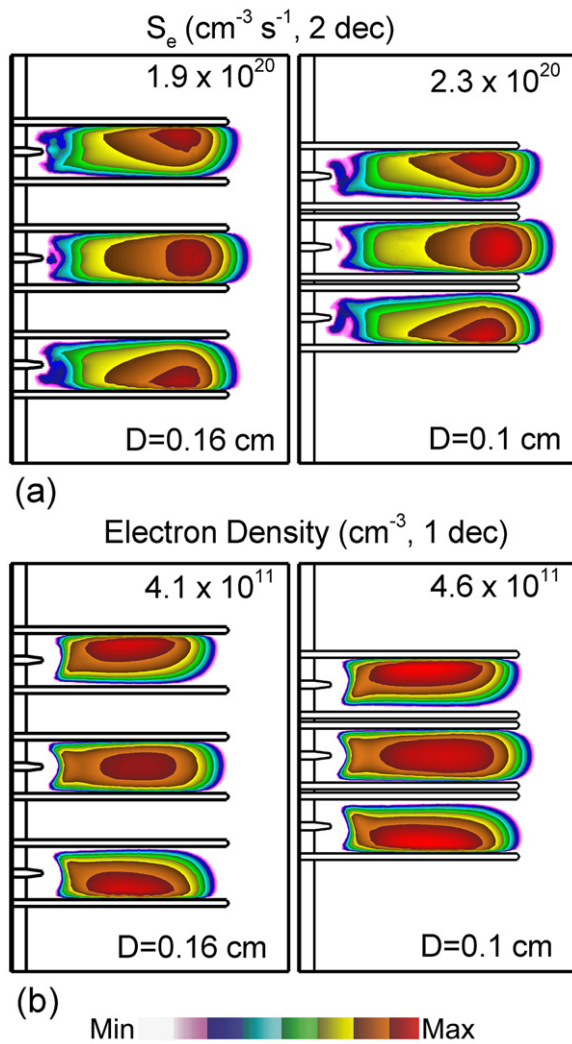


**Figure 12.** Close-up of (a) electron impact ionization source and (b) electron density inside the tubes for the three-jet array for tube separations of 0.16 and 0.105 cm.

interact, they are physically separate and propagate in what are independent He channels until those individual He channels are diffusively dispersed.

The electron impact ionization source, electron density and negative space charge for a three-jet array having the middle separation, 0.16 cm, are shown in figure 11. Close-ups of the electron impact ionization source and electron density inside the tubes are shown in figure 12. The peak electron densities ( $5 \times 10^{11} \text{ cm}^{-3}$ ) and ionization sources ( $3 \times 10^{20} \text{ cm}^{-3} \text{ s}^{-1}$ ) at 17 ns are similar inside the tubes to the three-jet array with medium separation. However, here the closer proximity of the jets magnifies the consequences of the electrostatic forces. These forces skew the electron density and ionization sources of the top and bottom tubes against their top and bottom walls while the electron density and ionization source of the middle tube is centered in the tube. These forces overcome the tendency of a single jet to propagate in a wall-hugging mode inside the tube.

Upon emerging from the tubes, the larger electrostatic forces push the top and bottom plasma bullets deeper into the low He mole fraction at the periphery of their channels. As a

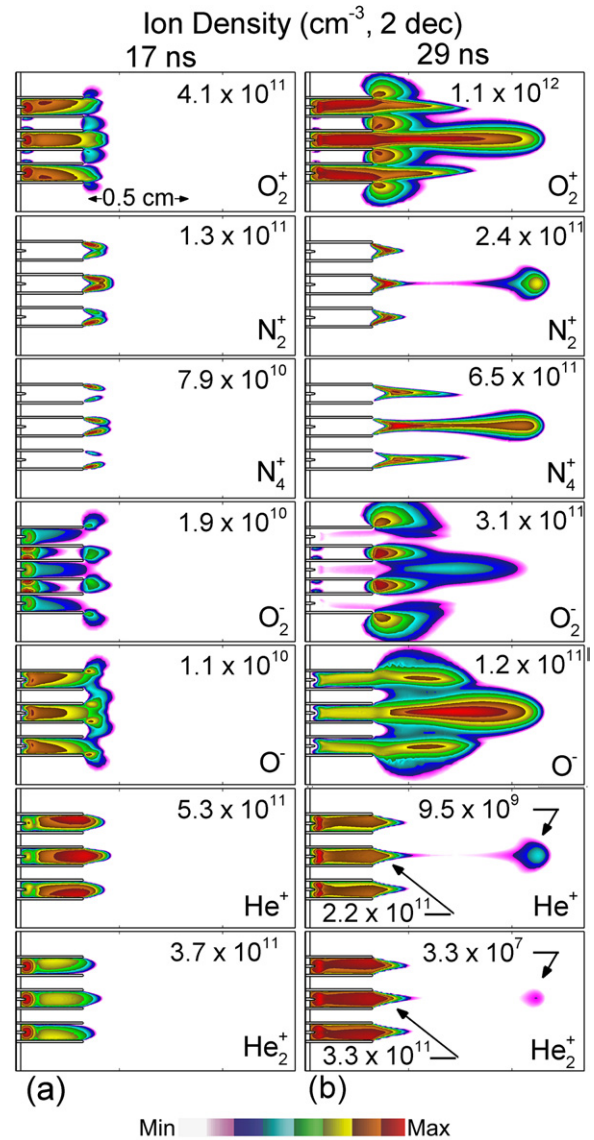


**Figure 13.** Ion densities for the three-jet array for medium separation ( $D = 0.16 \text{ cm}$ ) at (a) 17 ns (when the plasma bullets emerge from the tubes) and (b) 29 ns (when the IWs merge). Contours are plotted on a two-decade log scale with maximum densities shown in each frame.

result, the top and bottom IWs slow in speed and decay more rapidly compared with the center IW. This leaves the center plasma bullet with an electron density 20 times larger than its neighbors at 28 ns and propagating at about twice the speed. The top and bottom bullets do indeed die as the He channels merge. The top and bottom IWs fail to merge with the center IW, leaving only the center plasma bullet to propagate. In the absence of the confining forces of the top and bottom IWs, the middle IW expands to fill the He channel.

Ion densities for the three-jet array with a medium separation ( $D = 0.16 \text{ cm}$ ) at 17 ns (when the plasma emerges from the tubes) and 29 ns (when the plasma bullets merge) are shown in figure 13. The ion composition changes with time to reflect the changing composition of the gas plume. At 17 ns, within the tubes the dominant ions are  $\text{He}^+$  ( $5.3 \times 10^{11} \text{ cm}^{-3}$ ),  $\text{O}_2^+$  ( $4.1 \times 10^{11} \text{ cm}^{-3}$ ) and  $\text{He}_2^+$  ( $3.7 \times 10^{11} \text{ cm}^{-3}$ )

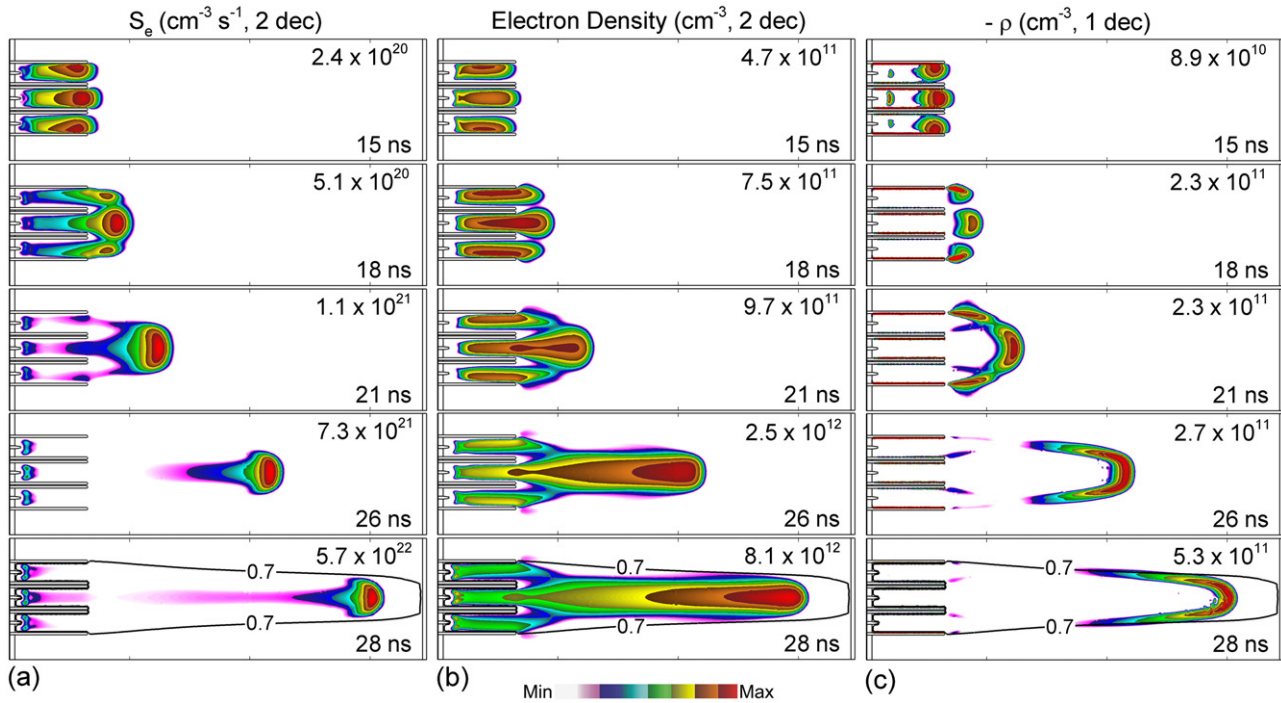


**Figure 14.** Plasma characteristics for a three-jet array with a close separation ( $D = 0.105$  cm) for times after the voltage is applied. (a) Electron impact ionization source, (b) electron density and (c) negative space charge. The contours are plotted on a log scale with the maximum value shown in each frame. The lines show the contour of 70% helium mole fraction.

with approximately the same densities. Note that despite the small mole fraction of  $O_2$  inside the tube, due to its lower ionization potential and Penning reactions, the  $O_2^+$  ion density is comparable to that of  $He^+$ .  $N_2^+$  ions are produced at the boundary of the He channels where the diffusion of  $N_2$  provides a sufficient density of collision partners and there are still enough energetic electrons and excited helium atoms (or  $He_2^*$ ) to ionize the  $N_2$ .

At 29 ns  $N_2^+$  ions ( $2.4 \times 10^{11} \text{ cm}^{-3}$ ) are produced in the head of the streamer by electron impact ionization in the increasing density of  $N_2$  as air diffuses into the plume. The  $N_2^+$  density is rapidly depleted by associative charge exchange to form  $N_4^+$  having a density of  $6.5 \times 10^{11} \text{ cm}^{-3}$ . A small density of  $He^+$  ( $9.5 \times 10^{10} \text{ cm}^{-3}$ ) is sustained by the IW though the decreasing density of He in the plume reduces the density of  $He_2^+$  ( $3.3 \times 10^7 \text{ cm}^{-3}$ ). At 29 ns, the  $O_2^+$  ions ( $1.1 \times 10^{12} \text{ cm}^{-3}$ ) have the largest density.

The  $O^-$  and  $O_2^-$  have roughly equal densities both inside and outside the tubes. The  $O^-$  density increases by about an order of magnitude ( $1.1 \times 10^{10}$  to  $1.2 \times 10^{11} \text{ cm}^{-3}$ ) from inside the tube into deep in the plume.  $O_2^-$  undergoes a similar increase ( $1.9 \times 10^{10}$  to  $3.1 \times 10^{11} \text{ cm}^{-3}$ ). The increases of both negative ions result from the increase in the mole fraction of  $O_2$  as air diffuses into the plume. The density of  $O_2^-$  is largest in the halos, whereas the density  $O^-$  is maximum in the IW channel. These trends result from the rate coefficient for three-body attachment to form  $O_2^-$  decreasing with electron temperature as  $T_e^{-1}$  whereas the rate coefficient for dissociative attachment to form  $O^-$  increases with electron temperature up to about 4 eV for these conditions. The electron temperature in the halo is about 0.5 eV, producing a negligible rate coefficient for attachment to form  $O^-$ , whereas in the head of the streamer,

the electron temperature is about 2.5 eV, resulting in a large rate coefficient for attachment ( $3 \times 10^{-11} \text{ cm}^3 \text{ s}^{-1}$ ).

Finally, the evolution of plasma properties for the closely spaced three-jet array is shown in figure 14. Close-ups of the electron impact ionization source and electron density inside the tube are shown in figure 12. As with the closely spaced two-jet array, the He plumes merge upon leaving the tubes. In this case, the jets interact through all of the electrostatic, fluid and photolytic processes. The proximity of the jets to each other produces severe electrostatic repulsion inside the tubes resulting from the individual negative space charge of each IW. Upon emerging from the tubes, the IWs encounter the single merged He channel. The top and bottom IW are steered by the high air mole fraction contours towards the center of the merged He channels. The ionization sources appear nearly fully merged by 21 ns (figure 14(a)), though the IWs do retain some aspect of individuality, as suggested by the electron density and space charge at 21 ns. Between 21 and 26 ns, the plasma bullets coalesce into the center of the merged He channel, leaving a single plasma plume. This process is enhanced by the photoionization from the top and bottom IWs, which increase the speed of propagation of the center IW.

Ion densities for the closely spaced three-jet array at 17 ns (when the plasma emerges from the tubes) and 27 ns (when the IWs merge) are shown in figure 15. The trends are similar to those shown in figure 13 for the medium spacing while reflecting the single helium channel. The  $He^+$  density ( $1.7 \times 10^{12} \text{ cm}^{-3}$ ) is here comparable to the density of  $N_2^+$  density ( $1.2 \times 10^{12} \text{ cm}^{-3}$ ),  $N_4^+$  density ( $9.8 \times 10^{11} \text{ cm}^{-3}$ ) and  $O_2^+$  density ( $8.7 \times 10^{11} \text{ cm}^{-3}$ ) in the merged channel. This reflects the slower rate of diffusion of air into the core of the merged He plume. The density of  $He_2^+$ , formed by reaction

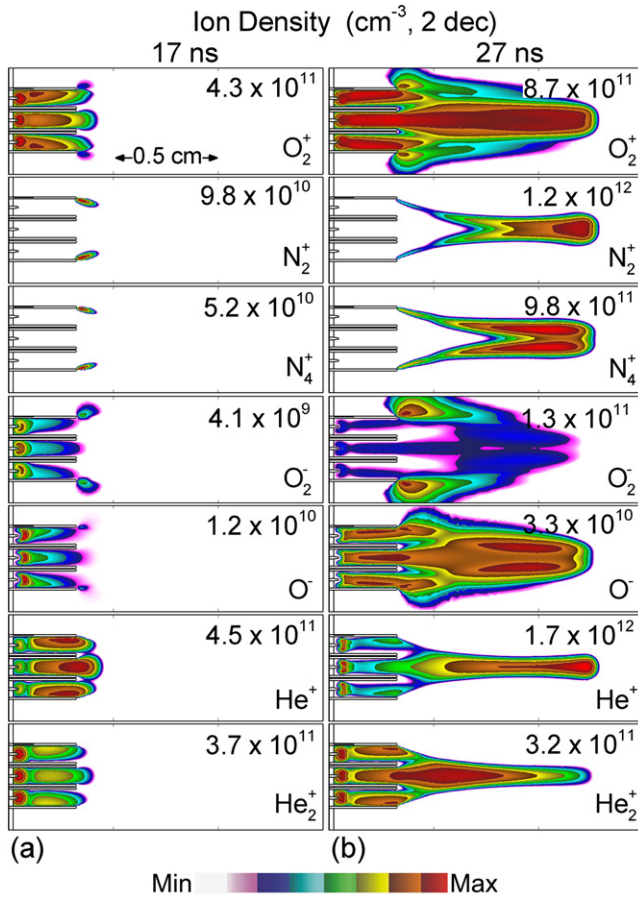


**Figure 15.** Ion densities for the three-jet array for a close separation ( $D = 0.105$  cm) at (a) 17 ns (when the plasma bullets emerge from the tubes) and (b) 27 ns (when the IWs merge). Contours are plotted on a two-decade log scale with maximum densities shown in each frame.

between  $\text{He}^+$  and  $\text{He}$ , is larger compared with  $\text{He}^+$  close to the tubes where the mole fraction of  $\text{He}$  is larger and more time has elapsed to allow for the associative charge exchange.  $\text{He}^+$  dominates in the merged IW channel. Note that the  $\text{N}_2^+$  density peaks in the center of the plume where the electron density is highest whereas the  $\text{N}_4^+$  density, formed by collisions between  $\text{N}_2^+$  and  $\text{N}_2$ , is maximum at the sides of the plume where the  $\text{N}_2$  density is higher. The same is true for  $\text{O}^-$ . The  $\text{O}_2^-$  density is maximum in the halo of the jet where low-energy electrons are produced by photoionization in a region of high  $\text{O}_2$  density. Note that the ion densities are generally larger compared with those shown in figure 13 for a medium separation. This is likely due to the larger rate of diffusion of air into the center  $\text{He}$  channel with the larger separation.

Our findings correlate well with experimental observations. For example, Kim *et al* [28] found that the outer quartz tubes in a hexagonal array of plasma jets did not produce strong individual plumes but instead reinforced the centered plasma plume, despite the presence of an equally distributed gas flow. In experiments by Nie *et al* [25], also using a hexagonal array of seven jets, the central jet was strongest in the negative half-cycle. Ghasemi *et al* [33] observed divergence of the outer plumes in an array of plasma jets, an effect attributed to electrostatic repulsion.

We included in our calculations the momentum transfer forces between the ions and the neutral gas flow and so there is momentum being imparted to the gas from the electrostatic repulsion between the IWs. Plasma–neutral flow interactions have been experimentally observed [53, 54]. For example, Sarron *et al* [53] found that the forces from the IW propagating through a  $\text{He}$  channel into air can delay the onset of turbulence. Foletto *et al* [54] found that the location downstream that turbulence occurs was affected by the plasma for  $\text{He}$  jets into air, more so at a lower Reynolds number. We did not observe significant effects on the  $\text{He}$  channels resulting from the plasma–plume interaction, which is most likely a result of our simulating a single pulse. These interactions likely require many pulses to produce.

These interactions also depend on the flow rate. For example, Kim *et al* [28] found that a hexagonal array of plasma jets strongly interacted with a low flow rate of 1–3.5 slm. When the gas flow rate was higher than 3.5 slm in these particular experiments, the plasma jets no longer interacted with each other, but rather transformed into well-collimated plasma plumes regardless of the operating voltage. Although not discussed in detail here, we have found similar trends in our modeling results. The higher the gas flow rate, the longer the individual  $\text{He}$  channels remain distinct prior to air diffusing into the channels or merging with adjacent channels. Another sensitive experimental variable is the ratio  $R$  of the plasma jet diameter to the jet–jet distance. Cao *et al* [27] found strong coupling between the jets was for ratios greater than  $R = 0.4$ , a value close to that observed in our simulations.

In the results just discussed, the voltage is simultaneously applied to all pin electrodes. This is likely the case for arrays of plasma jets where the same power supply is used for all electrodes. We did observe additional interactions between the jets if the voltage is not simultaneously applied. For example, we found that the center jet in a three-jet array could be diminished if the timing between the voltage applied to the outer jets is in a critical range. This interaction results from the conductive channels of the outer plasma jets extending the applied potential along their tubes, which then affects the center jet.

## 6. Concluding remarks

In this paper, we discussed results from a computational investigation of the properties of ionization waves (or plasma bullets) from one-, two- and three-plasma jet arrays.  $\text{He}/\text{O}_2$  mixtures were injected through tubes into flowing humid air. The properties of the plasma plumes largely depend on air diffusing into the jets of the  $\text{He}/\text{O}_2$  mixture. Large separation between the jets maintains unique  $\text{He}$  channels for longer distances. With synchronized voltage pulses, simultaneous plasma bullets are produced. Due to the negative space charge of the bullets, the heads of the IWs initially repel each other. As the spacing between the jets decreases, the gas flow fields begin to merge which, for sufficiently close jets, results in a merging of the IWs into a single plasma plume. These interactions between jets are sensitive functions of the gas flow rates, spacing between the jets and the timing of

voltage applied to each jet. Plasma jets (and jet arrays in particular) typically operate with an ac voltage, which produces ionization waves with both polarities. The choice of negative polarity for the results discussed here was intended to be illustrative of the possible interactions between jets. This choice likely minimizes the electrostatic interactions between jets. With positive polarity, stronger interactions between the streamers are expected (other conditions being equal) due to higher electric fields typically found in the positive streamer heads [39].

## Acknowledgments

We are grateful to Mr Peter Simon and Professor Annemie Bogaerts for their careful reading of the *nonPDPSIM* fluid modules and for their suggested updates. This work was supported by the US Department of Energy Office of Fusion Energy Science Contract DE-SC0001939 and the National Science Foundation.

## References

- [1] Kong M G, Kroesen G, Morfill G, Nosenko T, Shimizu T, van Dijk J and Zimmermann J L 2009 *New J. Phys.* **11** 115012
- [2] Morfill G E, Kong M G and Zimmermann J L 2009 *New J. Phys.* **11** 115011
- [3] Laroussi M, Mendis D A and Rosenberg M 2003 *New J. Phys.* **5** 41
- [4] Graves D B 2012 *J. Phys. D: Appl. Phys.* **45** 263001
- [5] Lu X, Laroussi M and Puech V 2012 *Plasma Sources Sci. Technol.* **21** 034005
- [6] Urabe K, Morita T, Tachibana K and Ganguly B N 2010 *J. Phys. D: Appl. Phys.* **43** 095201
- [7] Teschke M, Kedzierski J, Finantu-Dinu E G, Korzec D and Engemann J 2005 *IEEE Trans. Plasma Sci.* **33** 310
- [8] Lu X, Jiang Z, Xiong Q, Tang Z, Hu X and Pan Y 2008 *Appl. Phys. Lett.* **92** 081502
- [9] Walsh J L and Kong M G 2008 *Appl. Phys. Lett.* **93** 111501
- [10] Laroussi M and Lu X 2005 *Appl. Phys. Lett.* **87** 113902
- [11] Li Q, Li J T, Zhu W C, Zhu X M and Pu Y K 2009 *Appl. Phys. Lett.* **95** 141502
- [12] Stoffels E, Kieft I E and Sladec R E 2003 *J. Phys. D: Appl. Phys.* **36** 2908
- [13] Sands B L, Huang S K, Speltz J W, Niekamp M A, Schmidt J B and Ganguly B N 2012 *Plasma Sources Sci. Technol.* **21** 034009
- [14] Babayan S E, Jeong J Y, Tu V J, Park J, Selwyn G S and Hicks R F 1998 *Plasma Sources Sci. Technol.* **7** 286
- [15] Hemke T, Wollny A, Gebhardt M, Brinkmann R P and Mussenbrock T 2011 *J. Phys. D: Appl. Phys.* **44** 285206
- [16] Lu X and Laroussi M 2006 *J. Appl. Phys.* **100** 063302
- [17] Reuter S and Winter J 2012 *IEEE Trans. Plasma Sci.* **40** 2788
- [18] Mericam-Bourdet N, Laroussi M, Begum A and Karakas E 2009 *J. Phys. D: Appl. Phys.* **42** 055207
- [19] Kim J Y, Ballato J, Foy P, Hawkins T, Wei Y, Li J and Kim S-O 2011 *Biosensors Bioelectron.* **28** 333
- [20] Cao Z, Walsh J L and Kong M G 2009 *Appl. Phys. Lett.* **94** 021501
- [21] Foest R, Kindel E, Ohl A, Stieber M and Weltmann K D 2005 *Plasma Phys. Control. Fusion* **47** B525
- [22] Pei X, Wang Z, Huang Q, Wu S and Lu X 2011 *IEEE Trans. Plasma Sci.* **39** 2276
- [23] Eden J G and Park S J 2006 *Phys. Plasmas* **13** 057101
- [24] Sakai O, Sakaguchi T and Tachibana K 2007 *J. Appl. Phys.* **101** 073304
- [25] Nie Q Y, Cao Z, Ren C S, Wang D Z and Kong M G 2009 *New J. Phys.* **11** 115015
- [26] Ma J H, Shih D C, Park S-J and Eden J G 2011 *IEEE Trans. Plasma Sci.* **39** 2700
- [27] Cao Z, Nie Q, Bayliss D L, Walsh J L, Ren C S, Wang D Z and Kong M G 2010 *Plasma Sources Sci. Technol.* **19** 025003
- [28] Kim J Y, Ballato J and Kim S-O 2012 *Plasma Process. Polym.* **9** 253
- [29] Kim J Y and Kim S-O 2011 *IEEE Trans. Plasma Sci.* **39** 2278
- [30] Kim S-O, Kim J Y, Kim D Y and Ballato J 2012 *Appl. Phys. Lett.* **101** 173503
- [31] Furmanski J, Kim J Y and Kim S-O 2011 *IEEE Trans. Plasma Sci.* **39** 2338
- [32] Fan Q-Q, Qian M-Y, Ren C-S, Wang D and Wen X 2012 *IEEE Trans. Plasma Sci.* **40** 1724
- [33] Ghasemi M, Olszewski P, Bradley J W and Walsh J L 2013 *J. Phys. D: Appl. Phys.* **46** 052001
- [34] Brok W J, Bowden M D, van Dijk J, van der Mullen J J A M and Kroesen G M W 2005 *J. Appl. Phys.* **98** 013302
- [35] Sakiyama Y and Graves D B 2006 *J. Phys. D: Appl. Phys.* **39** 3451
- [36] Sakiyama Y and Graves D B 2006 *J. Phys. D: Appl. Phys.* **39** 3644
- [37] Sakiyama Y and Graves D B 2009 *Plasma Sources Sci. Technol.* **18** 025022
- [38] Naidis G V 2010 *J. Phys. D: Appl. Phys.* **43** 402001
- [39] Naidis G V 2011 *Appl. Phys. Lett.* **98** 141501
- [40] Naidis G V 2011 *J. Phys. D: Appl. Phys.* **44** 215203
- [41] Boeuf J-P, Yang L L and Pitchford L C 2013 *J. Phys. D: Appl. Phys.* **46** 015201
- [42] Breden D, Miki K and Raja L L 2012 *Plasma Sources Sci. Technol.* **21** 034011
- [43] Bhoj A N and Kushner M J 2007 *J. Phys. D: Appl. Phys.* **40** 6953
- [44] Xiong Z, Robert E, Sarron V, Pouvesle J-M and Kushner M J 2012 *J. Phys. D: Appl. Phys.* **45** 275201
- [45] Liu D X, Bruggeman P, Iza F, Rong M Z and Kong M G 2010 *Plasma Sources Sci. Technol.* **19** 025018
- [46] Murakami T, Niemi K, Gans T, O'Connell D and Graham W G 2013 *Plasma Sources Sci. Technol.* **22** 015003
- [47] Dorai R 2002 *PhD Thesis* Department of Chemical Engineering, University of Illinois at Urbana-Champaign
- [48] Van Gaens W and Bogaerts A 2013 *J. Phys. D: Appl. Phys.* **46** 275201
- [49] Sakiyama Y, Knake N, Schröder D, Winter J, Schulz-von der Gathen V and Graves D B 2010 *Appl. Phys. Lett.* **97** 151501
- [50] Karakas E, Koklu M and Laroussi M 2010 *J. Phys. D: Appl. Phys.* **43** 155202
- [51] Xiong R, Xiong Q, Nikiforov A Yu, Vanraes P and Leys C 2012 *J. Appl. Phys.* **112** 033305
- [52] Arrayas M, Betelu S, Fontelos M A and Trueba J L 2008 *SIAM J. Appl. Math.* **68** 1122
- [53] Sarron V, Robert E, Fontane J, Darny T, Riès D, Dozias S, Joy L and Pouvesle J-M 2013 Plasma plume length characterization 21st Int. Symp. on Plasma Chemistry—ISPC (Cairns, Australia, 5–9 August 2013)
- [54] Foletto M, Douat C, Fontane J, Joly L, Pitchford L C and Puech V 2013 Influence of a plasma jet on the hydrodynamics of a helium jet 31st Int. Conf. on Phenomena in Ionized Gases—ICPIG (Granada, Spain, 14–19 July 2013)